Experimental study and in-situ FBG monitoring of process-induced strains during autoclave co-curing, co-bonding and secondary bonding of composite laminates

Laure Moretti, Philippe Olivier, Bruno Castanié, Gérard Bernhart

Experimental study and in-situ FBG monitoring of process-induced strains during autoclave co-curing, co-bonding and secondary bonding of composite laminates

L. Moretti[a], P. Olivier[b], B. Castanié[b], G. Bernhart[a]

[a] *Institut Clément Ader (ICA), Université de Toulouse, CNRS, Mines Albi, UPS, INSA, ISAE-SUPAERO, Campus Jarlard, 81013 Albi CT Cedex 09, France*

[b] *Institut Clément Ader (ICA), Université de Toulouse, CNRS, Mines Albi, UPS, INSA, ISAE-SUPAERO, 3 rue Caroline Aigle, 31400 Toulouse, France*

A B S T R A C T

The geometric stability of bonded structural parts, such as self-stiffened panels, is a critical issue in aeronautics. However, autoclave curing and bonding of large complex integrated primary structures often induce distortions compromising their geometric stability. Composite cure-induced strains and distortions have been extensively studied in the literature but the influence of the adhesive on these distortions has often been overlooked. More experimental data are therefore necessary to properly understand its influence on process-induced strains and its behaviour during cure. The present paper reports a wide range of new experimental investigations showing the non-negligible influence of the adhesive on cure-induced distortions of composite assemblies. The experimental data presented include post-cure distortion measurements, optical microscope imaging, micro-tomography imaging and FBG in-situ strain monitoring during an autoclave bonding process. These experiments demonstrate the impact of the adhesive film behaviour and of the manufacturing bonding process on final distortions and strains of composite assemblies.

Keywords: Thermosetting resin, Cure behaviour, Process monitoring, Assembly

Introduction

Primary integrated composite structures like wing boxes or fuselages are now currently used in aeronautics. Specific properties of composite laminates made of carbon and thermosetting resins bonded with structural adhesive films enable large weight savings. However, some processes used to manufacture integrated structures may induce significant residual strains and stresses that will impact the geometry and properties of assemblies. Composite parts and structural adhesive films experience various multi-physical phenomena during their curing, which may compromise the geometric stability of assemblies, especially for large complex integrated structures such as stiffened panels.

During curing, epoxy resin based materials are subjected to various sources of process-induced strains. The influential parameters can be divided between intrinsic and extrinsic parameters [1]. The main intrinsic parameters are thermal expansion and chemical shrinkage, while extrinsic parameters are due to external phenomena like curing conditions and tool/part interactions.

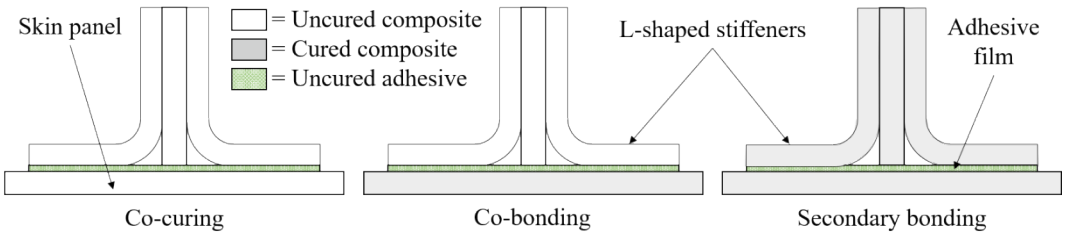

Fig. 1. Bonding processes used to manufacture integrated structures

Three main bonding processes can be used to manufacture integrated structures: co-curing, co-bonding and secondary bonding, as illustrated in Fig. 1. These bonding processes involve cured and uncured composite laminates and uncured adhesive films, the various substrates and adhesive films having different material properties. Such differences, especially those involving thermal expansion and chemical shrinkage, may induce some complex interactions between the various substrates of the assembly and generate cure-induced strains and stresses. The process-induced strains of autoclave-cured composite parts have been extensively studied in the literature [1–11] but the influence of the adhesive during autoclave-bonding of composite laminates has often been disregarded. However, research on aeronautic repair processes [12–14] and exterior automotive panels [15–20] have proved that adhesives may generate some noticeable strains for composite-metallic and composite-composite bonded assemblies. Some authors have studied the simulation of cure-induced strains and stresses of integrated composite material structures, but usually disregard the influence of the adhesive film [21,22].

The aims of the research work presented in this paper are to provide experimental data on process-induced strains that occur during bonding and curing of composite laminates and to produce new knowledge on the influence of adhesive films on the deformations of integrated structures at room temperature after curing. To do this, composite plates are bonded using co-curing, co-bonding and secondary bonding processes in an autoclave. Post-cure distortions (i.e. the distortions found at room temperature after curing) are measured and the states of the interface between the adhesive and the composite substrates are studied using optical microscope and micro-tomography imaging. In order to obtain better insight into the phenomena involved during the bonding cure of assemblies, in-situ strain monitoring is necessary during the cure. One of the less intrusive methods available nowadays is the use of optical fibre written with fibre Bragg grating (FBG) sensors. The successful use of such a sensor and its non-intrusiveness for in-situ monitoring has been proved in several studies on composite parts [6,23–29] and adhesives [30,31]. FBG sensors are therefore used here to monitor the development of cure-induced strains during a co-bonding process in an autoclave. To properly understand the influence of the adhesive on process-induced strains, two types of assemblies are

instrumented with FBG sensors: co-bonded laminates with adhesive films and co-bonded laminates without adhesive film (see Fig. 1).

2. Materials and experimental methods

2.1. Materials and manufacturing

To understand the behaviour of bonded composite assemblies during cure, specimens were manufactured using laminates made of a carbon/epoxy prepreg IMA/M21EV produced by Hexcel and FM300-M epoxy based structural adhesive films produced by Cytec. The IMA/M21EV prepreg is toughened with thermoplastic nodules. Adhesive films of the FM300 series are modified epoxy adhesive films and are available with three types of polyester carriers to improve the moisture resistance of the adhesive and reduce galvanic corrosion in metal/composite assemblies [32]. In the case of the FM300-M film, this carrier forms a random mat.

Table 1. Composite specimens manufactured

Sample name	**Stacking**	**Mould**
Cocure-Invar-0-4/4	$[0_4]^{uncured}$/FM300-M/$[0_4]^{uncured}$	*Invar*
Pl-Invar-0	$[0_8]$	*Invar*
Cocure-Invar-45-4/4	$[+45/-45]_2$/ FM300-M/$[-45/+45]_2$	*Invar*
Cocure-Invar-45-2/6	[+45/-45]/FM300-M/[+45/-45/-45/+45/-45/+45]	*Invar*
Pl-Invar-45	$[+45/-45]_{2s}$	*Invar*
Cocure-Alu-45-4/4	$[+45/-45]_2$/ FM300-M/$[-45/+45]_2$	Aluminium
Cocure-Alu-45-2/6	[+45/-45]/FM300-M/[+45/-45/-45/+45/-45/+45]	Aluminium
Pl-Alu-45	$[+45/-45]_{2s}$	Aluminium
Cobond-Invar-0-20-1a	$[0_{20}]^{cured}$/FM300-M/$[0_{20}]^{uncured}$	*Invar*
Cobond-Invar-0-20-2a	$[0_{20}]^{cured}$/FM300-M_2/$[0_{20}]^{uncured}$	*Invar*
Cobond-Invar-0-20-0a	$[0_{20}]^{cured}$/$[0_{20}]^{uncured}$	*Invar*
Cocure-Invar-0-20	$[0_{20}]^{uncured}$/ FM300-M/$[0_{20}]^{uncured}$	*Invar*
SecBond-Invar-0-20	$[0_{20}]^{cured}$/ FM300-M/$[0_{20}]^{cured}$	*Invar*
Pl-Invar-0-20	$[0_{20}]$	*Invar*

The composite laminates were cured and bonded through an autoclave process using a two-dwell temperature cycle achieving 180°C during the second and highest dwell (the complete cure cycle is shown in Fig. 11). Depending on the bonding process used, the laminates underwent one or two identical curing cycles since, in the case of the co-bonding process, the skin panels underwent the same cure cycle twice. The panel was cured alone during the first cycle and then passed to the second one, which cured the uncured laminate and the adhesive film. The laminates and assemblies were manufactured on *Invar* or aluminium moulds treated with FREKOTE 700C liquid release agent and

protected with an FEP releasing film. Thick and thin laminates, 150 mm x 150 mm, were bonded using the various processes: co-curing, co-bonding and secondary bonding as summarized in Table 1.

2.2. Post-cure experimental measurements

Post cure distortions were measured after demoulding at ambient temperature for each specimen described in Table 1. Final distortions of the parts were obtained using Stereo-Digital Image Correlation (S-DIC) [33,34]. Speckles necessary for the S-DIC were painted on the laminate surfaces that were in contact with the mould during curing. S-DIC measurements were performed using two Allied Vision Pike F-505B/F505-C cameras and three-dimensional profiles of the specimens studied were reconstructed using VIC3D software.

To obtain a better understanding of the bonding processes, and of the influence of the adhesive and its interfaces with the laminates, optical microscope imaging and micro-tomography imaging were also performed on the bonded specimens. X-Ray 3D-micro-computed tomography images were obtained using an EasyTom 130 Micro-Tomography scanner from RX Solutions. The associated RX Solutions X-Act 2.0 software was used for post-processing.

2.3. Methodology and experimental set-up for FBG in-situ monitoring

Fibre Bragg gratings (FBG) are one of the least intrusive sensors available for making in-situ measurements in composite materials. They present several advantages, such as the small diameter of the optical fibre, the good sensitivity of the sensor and the possibility of writing multiple gratings on a single optical fibre, thus allowing distributed strain measurements.

Optical fibres are composed of a dielectric core covered with an optical sheath usually made of silica, and single-mode optical fibres are generally used for in-situ monitoring. A fibre Bragg grating (FBG) is a micro-structure written on the core of the optical fibre, which generates a periodic modification of the refractive index along a small segment of the optical fibre, generally a few millimetres long. The Bragg grating of an optical fibre connected to a broadband source of light reflects back a narrow band of light around a singular peak corresponding to the central wavelength of reflexion, also called the Bragg wavelength and noted λ_B. The Bragg wavelength depends on the refractive index n_{eff} as defined in equation (1) [35,36].

$$\lambda_B = n_{eff} \cdot \Lambda \qquad (1)$$

where Λ is the period of the grating, n_{eff} is the core effective refractive index and λ_B is the Bragg wavelength.

Any variation in the period step of the Bragg grating or of the effective reflective index results in a proportional change in the reflected wavelength. These two variables can be influenced by strain, temperature, and pressure. The influence of pressure on the Bragg wavelength variation has been shown to be negligible during an autoclave process

[28] so, as long as the maximum applied autoclave pressure does not exceed 1 MPa, the changes in the Bragg wavelength can be related to strain and temperature using equation (2) [35,36].

$$\frac{\Delta\lambda_B}{\lambda_B} = (\alpha_{of} + \xi_{of}) \cdot \Delta T + (1 - p_e) \cdot \varepsilon = K_T \cdot \Delta T + K_\varepsilon \cdot \varepsilon \qquad (2)$$

where α_{of} is the coefficient of thermal expansion of the optical fibre, ξ_{of} is its thermo-optic coefficient and p_e is the strain-optic constant. $K_T = \alpha_{of} + \xi_{of}$ and $K_\varepsilon = 1 - p_e$ are respectively the temperature and the strain sensitivity of the Bragg grating sensor. ΔT is the variation of the temperature around the FBG and ε is the axial strain along the FBG. For the optical fibres used in this paper $K_T = 7.6 \cdot 10^{-6}\,°C^{-1}$ and $K_\varepsilon = 0.782 \cdot 10^{-6}\,\mu\varepsilon^{-1}$ [40].

An embedded FBG sensor will generally be subjected to temperature variations and mechanical stresses at the same time. In order to decorrelate the temperature variation from the axial strains measured by the FBG, various methods have been used in the literature, such as: core dopants [24,25], calibration and combined measurements with embedded thermocouples [6,23,38], and encapsulated sensors [27,28,31,39]. In this research, it was decided to encapsulate a calibrated FBG at the end tip of each optical fibre to obtain in-situ temperature measurements and to decorrelate the thermal effect from the axial strain measurements. End tip FBGs were encapsulated following the experimental method used by Mulle et al. [28].

Bragg grating fibres used for this research were produced by iXblue Photonics. Each was written with four Bragg gratings, the end tip one being encapsulated as described above. The configuration used for the optical fibres is illustrated in Fig. 2. The length of the fibre destined to be embedded inside the composite or the adhesive was completely bare so that contact with the surrounding material was as direct as possible. The rest of the fibre was protected by a polyimide coating able to withstand curing temperatures without undergoing any degradation. The last two metres of fibre were located outside the autoclave and protected by a supplementary buffer. Finally, the fibres were equipped with FC/APC plugs to connect the optical fibres to a MicronOptics Si425 wavelength interrogator. As shown in [37], the stresses development during the curing of unidirectional laminates does not induce any changes in the optical signal spectrum. This is why the analysis was carried out only with a wavelength interrogator and no spectrum analyser.

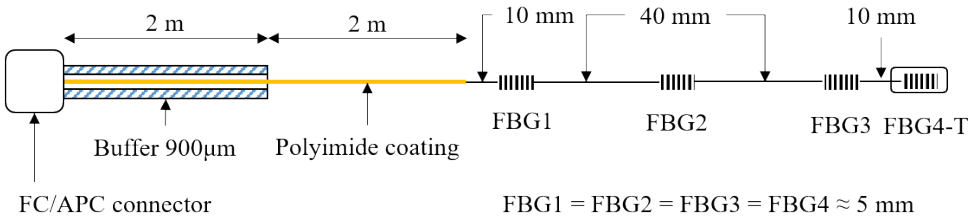

Fig. 2. Configuration of optical fibres – Uncoated fibre diameter = 125 µm.

The experimental set-up used to monitor process-induced strains during the autoclave cure cycle is illustrated in Fig. 3 and was inspired by work carried out by Mulle et al. [27,28,40]. The objective of the in-situ strain monitoring presented in this paper was to better understand the influence of adhesives on cure-induced strains. For this purpose, strain gradients developed in the thickness and in the plane of two types of co-bonded specimens, one with adhesive and one without, were monitored and compared. The co-bonded specimens, instrumented with FBG, were assemblies of two plates composed of 20 plies [0_{20}] of M21EV/IMA having dimensions 150 x 150 mm, one with two FM300-M adhesive films and one with no adhesive film. The FBG instrumentation of the two co-bonded assemblies is illustrated in Fig. 4. The first optical fibre, called OF_1, was placed either between the two adhesive films or between the uncured and cured composite laminates, depending on the assembly configuration considered. The three other fibres were embedded in the uncured composite laminate: one (called OF_2) between the first and second plies, one (called OF_3) in the middle of the laminate between the tenth and eleventh plies, and one (called OF_4) between the penultimate and the last plies. Optical fibres were embedded parallel to the carbon fibres of the prepreg to avoid the resin accumulation observed by some authors [27,38] when the optical fibres were used perpendicularly to reinforcement fibres.

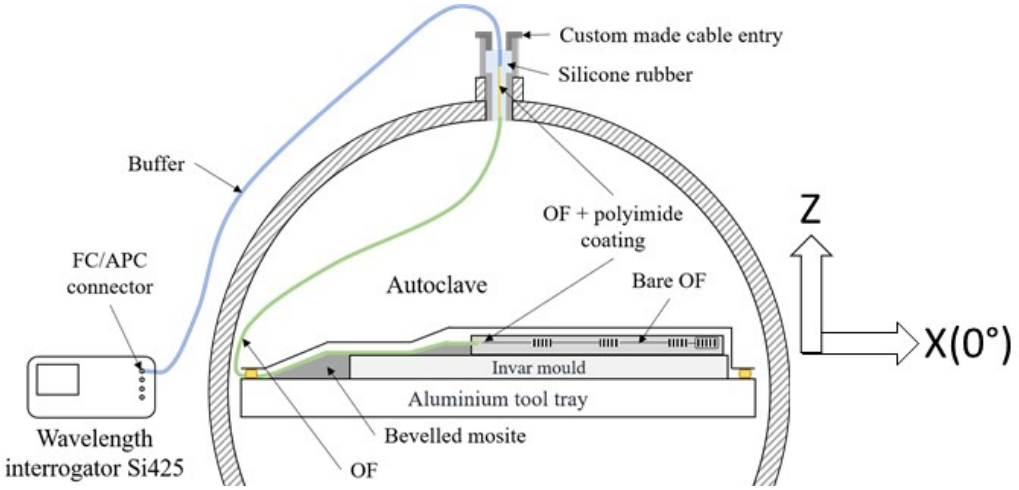

Fig. 3. Experimental set-up used for the cure monitoring during an autoclave cure

This experimental set-up enabled strain gradients in the thickness of the uncured composite laminates and the adhesive films to be measured. In addition, each optical fibre was written with four Bragg gratings to measure the strain gradients in the plane of the co-bonded specimens. The gratings were positioned to obtain strain measurements at the edge of the assemblies using FBG1, at the middle of the assemblies using FBG2 and at a quarter of the distance between the assembly edges (referred to as a quarter of the assembly hereafter) using FBG3. The FBG4-T grating was encapsulated to serve as a reference as explained above so that the effect of the temperature variation on the optical fibres could be subtracted. This last fibre Bragg grating was also used to measure the laminate and adhesive temperatures in situ. Exact locations of each FBG are detailed in Fig. 4(b).

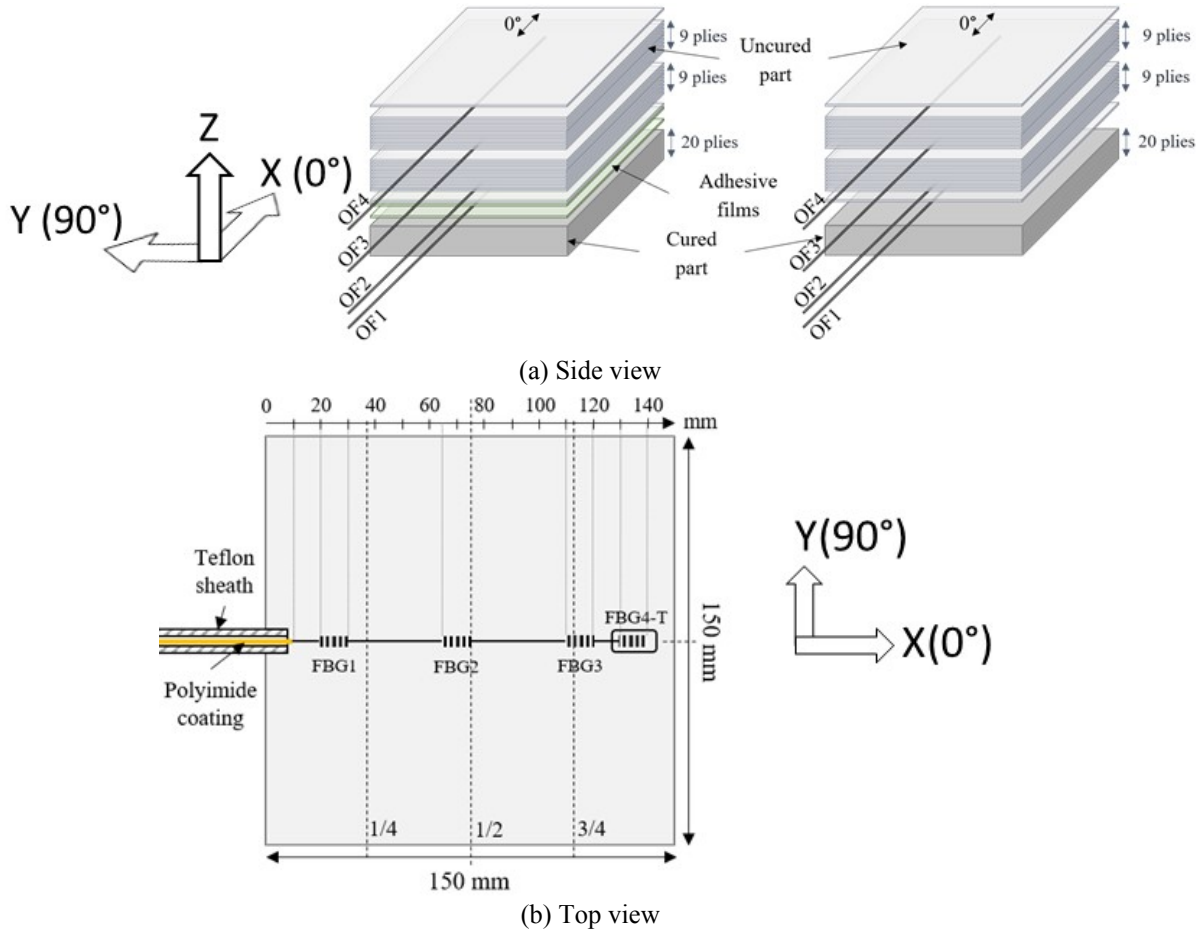

Fig. 4. FBG sensor locations in both assemblies

2.4. Thermomechanical Analysis

To verify the validity of the FBG in-situ measurements, Thermal Mechanical Analyses (TMA) were conducted on a Netzsch TMA 402 F3 Hyperion device. The samples used for the TMA tests were cut from a cured unidirectional laminate made of M21EV/IMA and a cured laminate of FM300-M films. All samples had final dimensions of 6 mm x 8 mm x 8 mm and were tested using a TMA force probe of 1 mN.

Three unidirectional samples of M21EV/IMA were tested on the TMA according to the direction of the reinforcement fibres. They were heated at 2°C/min from 20°C to 300°C and then cooled back down to 20°C at a rate of 2°C/min. This cycle was repeated twice for each sample. Further details upon the method and results obtained with these measurements are available in a previous paper [9].

On the other hand, three samples of FM300-M were tested on the TMA according to the thickness direction. They were heated at 2°C/min from 20°C up 270°C and then cooled back down to 20°C at a rate of 2°C/min. This cycle was also repeated twice for each sample.

The coefficients of thermal expansion obtained for the glassy laminates will be compared to post-cure measurements obtained by the embedded FBGs during heating ramps later in this paper (see Fig. 22). This comparison will validate the FBG in-situ monitoring method.

3. Sample warpage measured at room temperature after curing

Distortions of all specimens were measured at room temperature after curing by S-DIC on the laminate surface that was in contact with the mould during cure, as detailed in the Materials and experimental methods section. This method gives the complete post-cure distortion profile measured at room temperature after their curing. Using these profiles, the maximum out-of-plane deflection on the mould side was calculated and defined as warpage. The warpages measured for each specimen are summarized in Table 2. The warpage values presented were obtained on a single sample for each kind of specimen. More measurements will be needed in future works to validate the good repeatability of the process.

Table 2. Warpage measured by S-DIC at room temperature after curing

Sample name	Stacking	Warpage (mm)
Cocure-Invar-0-4/4	$[0_4]^{uncured}$/ FM300-M/$[0_4]^{uncured}$	0.979
Pl-Invar-0	$[0_8]$	0.488
Cocure-Invar-45-4/4	$[+45/-45]_2$/ FM300-M/$[-45/+45]_2$	0.967
Cocure-Invar-45-2/6	[+45/-45]/FM300-M/[+45/-45/-45/+45/-45/+45]	0.449
Pl-Invar-45	$[+45/-45]_{2s}$	0.255
Cocure-Alu-45-4/4	$[+45/-45]_2$/ FM300-M/$[-45/+45]_2$	1.170
Cocure-Alu-45-2/6	[+45/-45]/FM300-M/[+45/-45/-45/+45/-45/+45]	0.549
Pl-Alu-45	$[+45/-45]_{2s}$	0.488
Cobond-Invar-0-20-1a	$[0_{20}]^{cured}$/FM300-M/$[0_{20}]^{uncured}$	0.635
Cobond-Invar-0-20-2a	$[0_{20}]^{cured}$/FM300-M_2/$[0_{20}]^{uncured}$	0.514
Cobond-Invar-0-20-0a	$[0_{20}]^{cured}$/$[0_{20}]^{uncured}$	1.250
Cocure-Invar-0-20	$[0_{20}]^{uncured}$/ FM300-M/$[0_{20}]^{uncured}$	0.395
SecBond-Invar-0-20	$[0_{20}]^{cured}$/ FM300-M/$[0_{20}]^{cured}$	0.495
Pl-Invar-0-20	$[0_{20}]$	0.400

3.1. Results and analysis of the influence of the adhesive on thin laminates

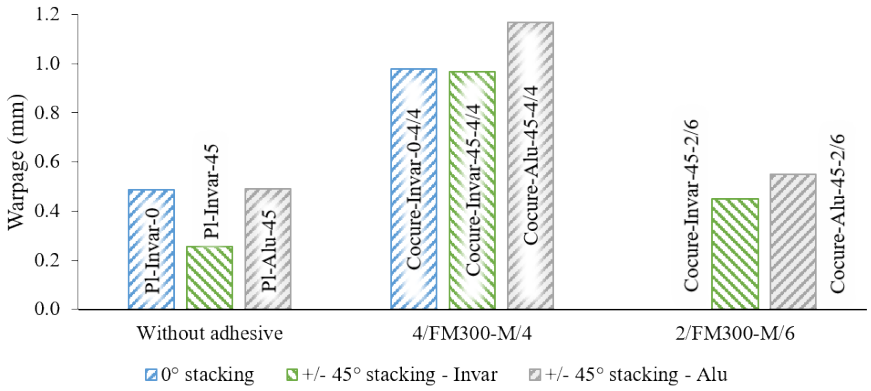

Fig. 5. Influence of the adhesive film on the final warpage of thin co-cured specimens

The warpage results obtained for thin co-cured specimens are illustrated in Fig. 5. Once an adhesive film is used, significant distortions are observed, even when the assembly is perfectly balanced. These balanced assemblies present warpages almost twice that of the same balanced laminates without adhesive and even greater warpage than unbalanced 2/FM300-M/6 assemblies. Observation of the upper surfaces of the co-cured laminates (vacuum bag side during cure) with the naked eye reveals some stains suggesting a migration of the adhesive. To gain a better understanding of the phenomena involved, the co-cured laminates were studied using micro-tomography and optical microscope imaging.

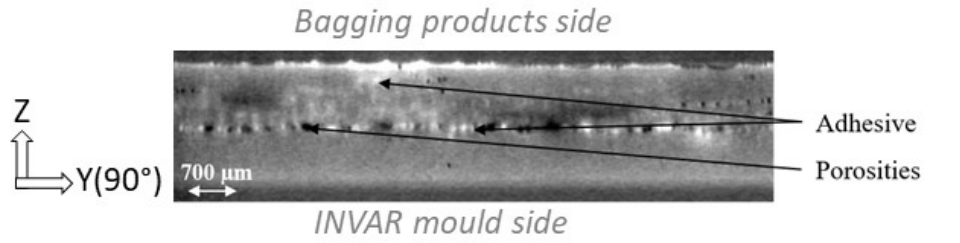

(a) Xrays microtomography

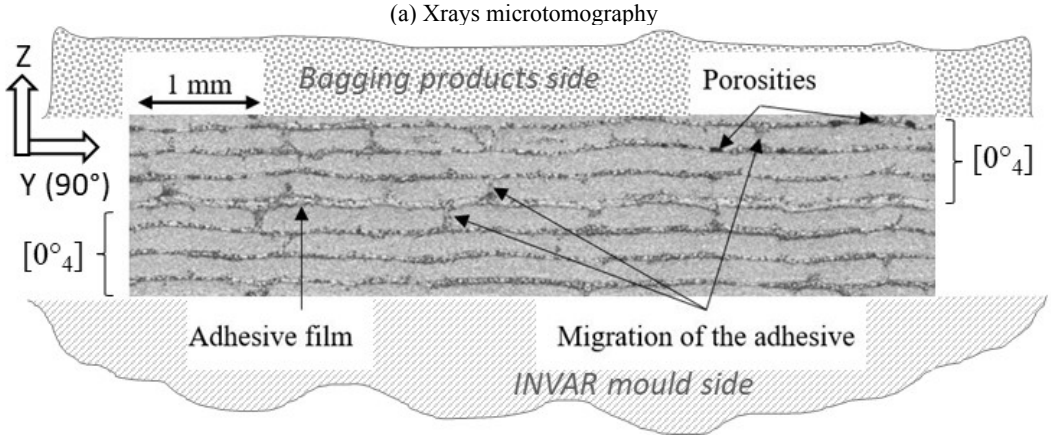

(b) Optical microscopy

Fig. 6. Micro-tomography images of a thin co-cured assembly “Cocure-Invar-0-4/4”

Micro-tomography images were taken on the co-cured thin laminate "Cocure-Invar-0-4/4". The results obtained in the plane directions perpendicular to the fibres (direction 1) and parallel to the fibres (direction 2) are illustrated in Fig. 6. These images suggest that the adhesive migrates in the upward direction perpendicular to the lamination plane and then infiltrates the upper plies of the laminates. The adhesive film, when migrating, generates porosities in the top laminate, which are partially filled by adhesive resin. The adhesive resin agglomerates visible with the naked eye on the top surface of the specimen can also be seen in tomography images. The adhesive mainly migrates to the vacuum bag-side laminate. As a result, most material properties, including the mechanical properties of the top laminate, are affected, generating or compensating for distortions. In the case of a perfectly balanced specimen, the assembly becomes asymmetrical and the adhesive resin migration induces serious warpage. Conversely, in the case of 2/FM300-M/6 co-cured assemblies (i.e. specimens Cocure-Invar-45-2/6 and Cocure-Alu-45-2/6), the stacking is already asymmetrical, and the adhesive resin migration then compensates for this asymmetry and reduces the warpage.

3.2. Results and analysis of the influence of the adhesive on thick unidirectional laminates

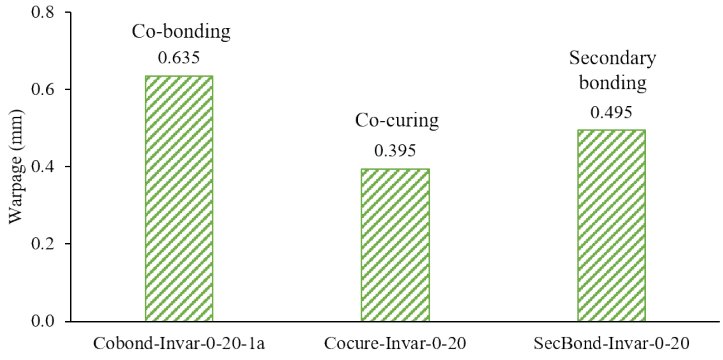

Fig. 7. Influence of the bonding process used on final warpage of assemblies of unidirectional laminates

Adhesive films and the migration of their resin have a strong influence on cure distortions of thin co-cured laminates. Cases of thicker bonded unidirectional laminates (two laminates of 20 plies and 0°) and the influence of the various bonding processes are now analysed.

The comparison of cure-induced distortions based on the bonding processes used co-curing, co-bonding or secondary bonding as illustrated in Fig. 7. We recall that each assembly was made with two 150 x 150 mm laminates of 20 plies each [0_{20}]. The laminates used for assemblies were cured on *Invar* moulds using the curing cycle described in the *Materials and manufacturing* section (see also Fig. 11). The three bonding processes were conducted on a single *Invar* mould during the same curing cycle. In the case of co-bonded specimens, the cured plate was systematically used as the bottom laminate for the assembly, i.e. was placed in contact with the mould during the cure cycle.

In the aim of better understanding the differences between processes, distortion profiles measured by S-DIC for each type of assembly are shown in Fig. 8. These profiles show that each of the bonding processes generates distortions for different reasons. The case of secondary bonding is the simplest: symmetrical laminate distortions are mainly caused by interaction between the mould and the part. The warpage observed on the secondary bonded assembly corresponds to the warpage induced for the [0_{20}] cured laminates used for the bonding process and, as shown in Table 2, the final warpage of these laminates (i.e. Pl-Invar-0-20) is almost the same as for secondary bonded assemblies (i.e. SecBond-Invar-0-20).

In the case of the co-curing process, on a thickness of 40 uncured plies, the influence of the mould is almost negligible. It is therefore probable that the slight dissymmetry of properties induced by the migration of the adhesive is the main factor inducing the distortions. This is consistent with the fact that the distortion profile illustrated in Fig. 8(b) is completely different from the one obtained on secondary bonded specimens. On the other hand, this profile is similar to distortion profiles obtained for co-cured thin balanced specimens (i.e. Cocure-Invar-0-4/4).

Finally, in the case of the co-bonding process, it is the dissymmetry generated by the difference in behaviour between the cured and the uncured laminates that generates most of the stresses and strains responsible for the final distortions.

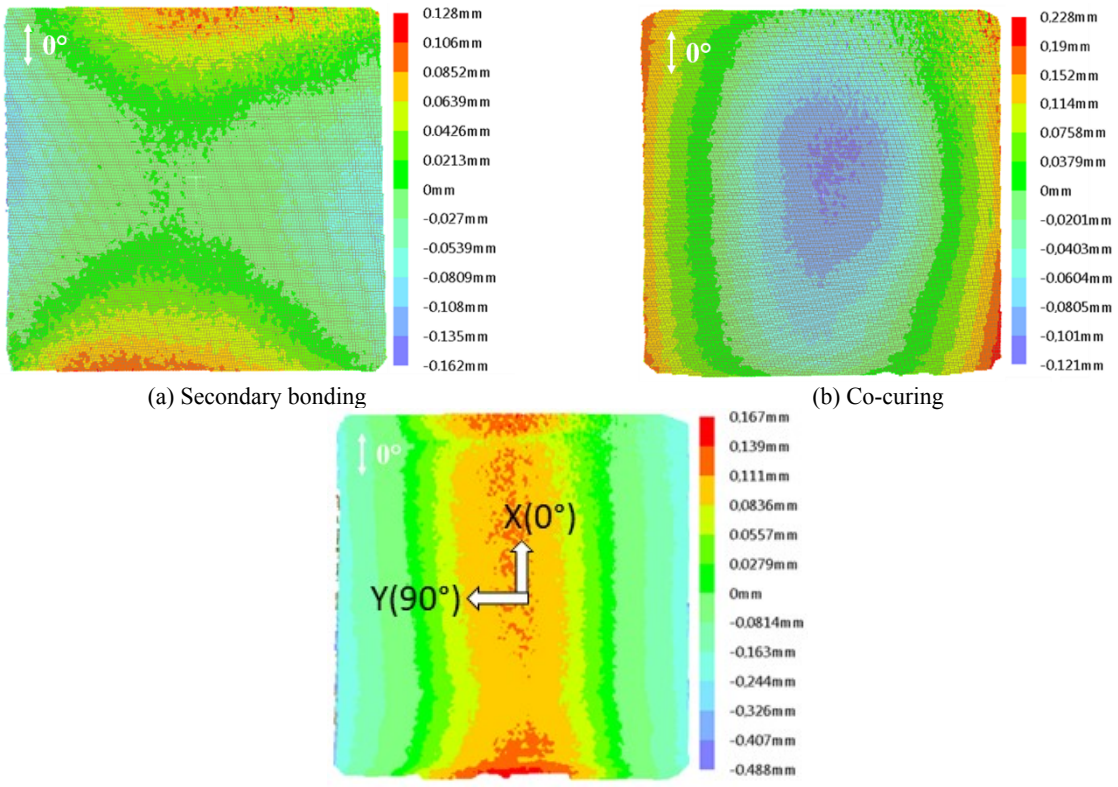

(a) Secondary bonding (b) Co-curing

(c) Co-bonding

Fig. 8. Post-cure distortion profile for each bonding process, measured by S-DIC.

To obtain more specific information about adhesive/composite interfaces generated during these bonding processes, images were obtained using tomography on the three types of bonded specimens, as illustrated in Fig. 9.

Fig. 9(b) illustrates the kind of images obtained by tomography for co-cured specimens. The migration effect of the adhesive seems to be better distributed within this assembly than within thin laminate assemblies. It is only visible in the first prepreg plies near the adhesive film and appears to occur in both upper and lower laminates. Therefore, the adhesive seems to have a less marked influence on the distortions than it would in thin assemblies. Nevertheless, the distortion profile shown in Fig. 8(b) confirms that the adhesive migration generates a slight dissymmetry. However, even with this slight dissymmetry, co-cured assemblies "Cocure-Invar-0-20" still exhibit the lowest warpages after demoulding of the three types of bonding processes.

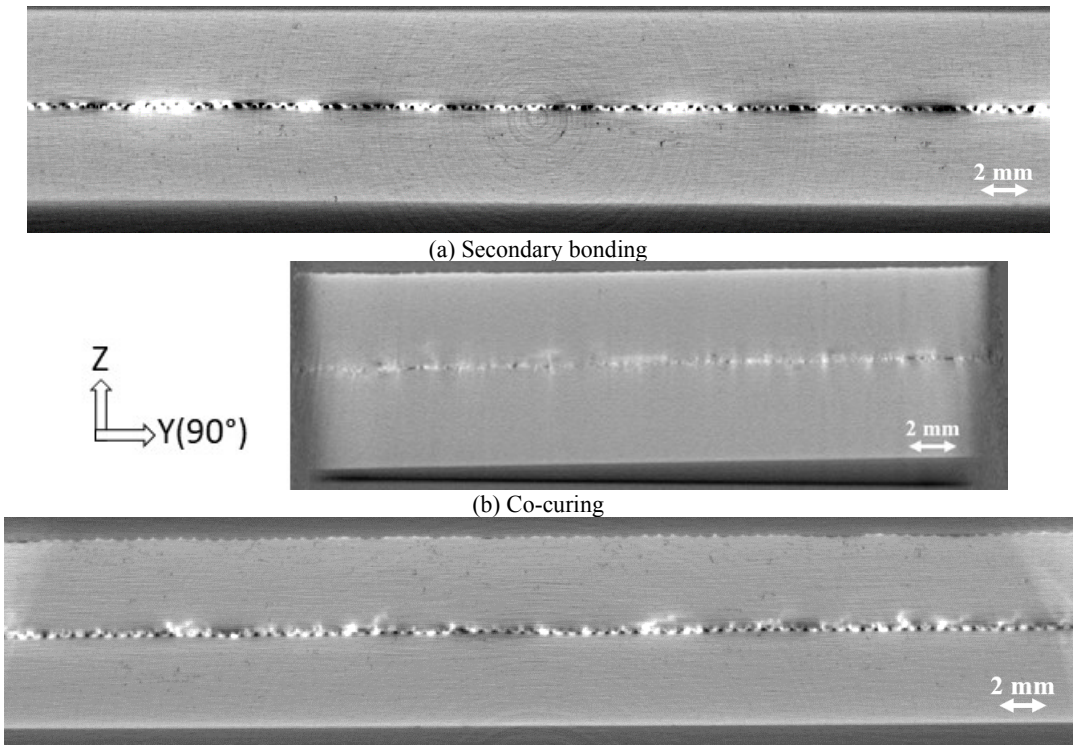

(a) Secondary bonding

(b) Co-curing

(c) Co-bonding

Fig. 9. Micro-tomography imaging of the bonded specimens of $[0_{20}]$ laminates

Interfaces seem more chaotic for laminates bonded by co-bonding and secondary bonding processes. Porosities appear within the adhesive with a regular pattern that corresponds to the peel ply fabric. It is visible in Fig. 9(c) on the side of the cured laminate for co-bonded assembly and on both sides in Fig. 9(a) for the secondary bonded assembly. In addition, for co-cured laminates, the adhesive migration occurs only on the side of the uncured laminate, but more consistently than during co-curing since the adhesive resin has only this path of migration.

The co-bonding process is one of the most commonly used process for manufacturing integrated structures such as self-stiffened panels in aeronautics. Particular attention was therefore paid to co-bonded assemblies. Warpage of specimens with one, two or no adhesive films was measured and the impact of the number of adhesive films is

illustrated in Fig. 10. It appears that, as the number of adhesive films increases, warpage decreases. The adhesive film enables a better distribution of stresses at the interface between cured and uncured laminates, resulting in a decrease of the final warpage of the part.

These results gave us important information on the distortions undergone by co-bonded, co-cured and secondary bonded laminates and measured after curing at room temperature. However, to properly understand the phenomena involved during curing, in-situ monitoring during an autoclave bonding process is necessary.

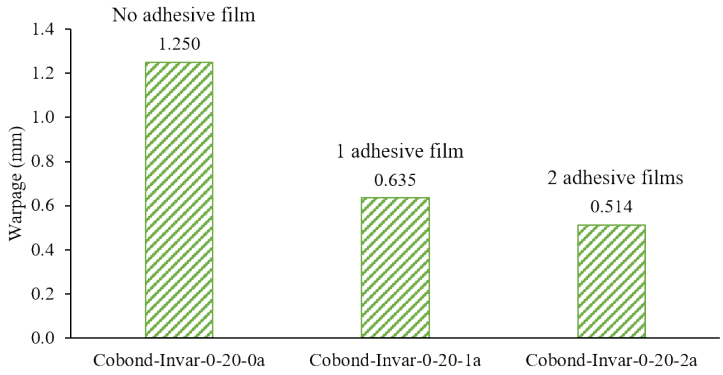

Fig. 10. Influence of the number of adhesive films on the final warpage of co-bonded specimens

4. FBG monitoring results

As already described in subsection 2.3, two unidirectional laminates of 20 plies [0_{20}] were instrumented with optical fibres (as illustrated in Fig. 4) and co-bonded during an autoclave curing cycle using two adhesive films for the first specimen and no adhesive film for the second one. Unfortunately, due to a handling incident, optical fibres OF_4 embedded between the penultimate and the last plies (see Fig. 4) were unable to measure strains properly for either specimen.

4.1. Temperature measurements and encapsulation control

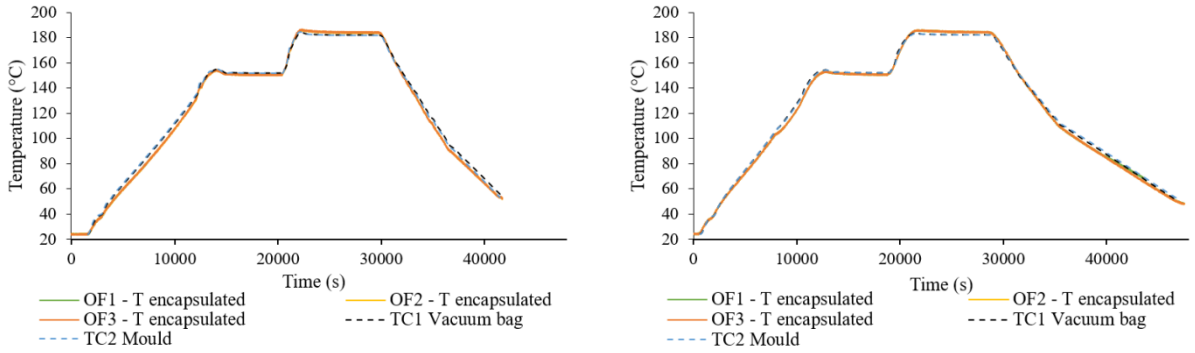

(a) specimen with adhesive films (a) specimen without adhesive film

Fig. 11. Temperature measurement during co-bonding obtained by thermocouples and by encapsulated FBG4-Ts

The temperature measured using each FBG4-T (encapsulated Bragg grating, see Fig. 4) and calculated using equation (3) was compared to the temperature measured by thermocouples placed on the top of the laminates and on the mould.

$$T = T_i + \Delta T = T_i + \frac{\Delta\lambda_{B4}}{\lambda_{B4} \cdot K_T} \qquad (3)$$

where λ_{B4} is the wavelength of encapsulated fibre Bragg gratings FBG4-T, T_i is the initial temperature at the beginning of the measurement and K_T is the temperature sensitivity of the fibres.

According to cure kinetics results obtained on the IMA/M21EV system [9], $[0°_{20}]$ laminates should not experience very great temperature gradients and the temperature measured by FBGs embedded in the uncured laminate should be close to those measured by thermocouples at the top of the assembly. Results obtained are given in Fig. 11. Measurements using the two techniques are consistent, the encapsulation of FBG4-T is therefore functional throughout the curing cycle, and process-induced strains can thus be obtained by subtracting the thermal effect from the in-situ measurements made by FBGs.

4.2. Adhesive and prepreg thermo-kinetic behaviour

To properly understand and analyse the strain measurements provided by FBGs, it is necessary to know the main thermo-kinetic behaviours of the adhesive and the prepreg. A thorough study of the prepreg and adhesive behaviours has been presented in previous works [9,36]. However, to simplify the study of the strain measurements presented in this paper, the thermo-kinetic behaviour of the materials is illustrated in Fig. 12. The results presented were obtained using various characterization procedures and a validated simulation tool. All the details are available and thoroughly described in previous works [9,36]. The gel points of the adhesive and the prepreg are pointed out as this information is especially significant for the following analysis of FBG measurements; before the gel points, the continuity of displacements between the materials and the optical fibres is not guaranteed.

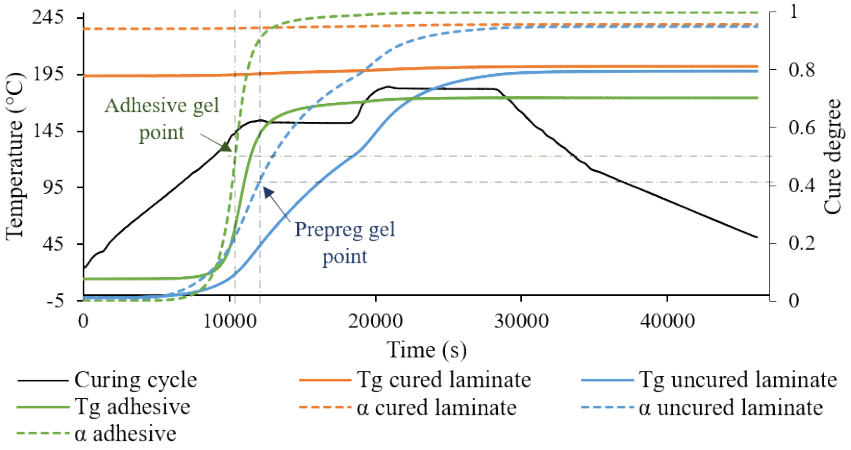

Fig. 12. Thermo-kinetic behaviours of the adhesive and the cured and uncured prepreg during the co-bonding process

4.3. Strain measurements for each optical fibre

Fig. 13(a) and (b) illustrate the development of strains measured by all OF_1 gratings placed, for the first specimen (Fig. 13(a)), between the two adhesive films or, for the second specimen (Fig. 13(b)), between the cured and the uncured laminates. Fig. 13(c) and (d) illustrate the development of strains measured by all OF_2 gratings positioned between the 1st and 2nd plies of the uncured laminates, and Fig. 13(e) and (f) illustrate the development of strains measured by all OF2 gratings positioned between the 10th and 11th plies of uncured laminates for both specimens. We recall that FBG1s were positioned at the edge of plies, FBG2s at the centre of the plies and FBG3s at a quarter of the plies (see Fig. 4). Note that, due to some experimental issues, FBG3 measurements of the OF_3 of the specimen co-bonded without adhesive were not exploitable.

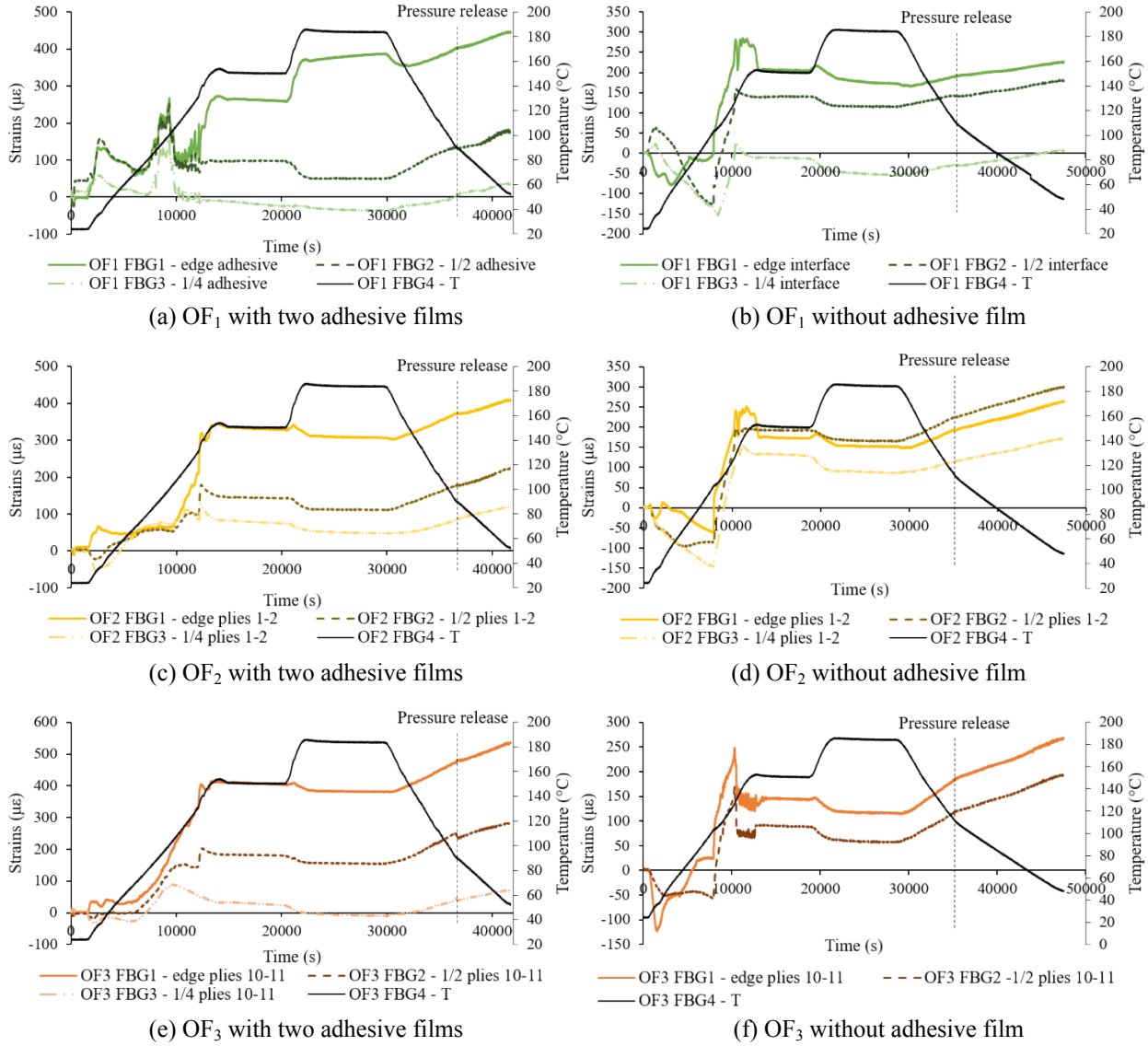

(a) OF_1 with two adhesive films

(b) OF_1 without adhesive film

(c) OF_2 with two adhesive films

(d) OF_2 without adhesive film

(e) OF_3 with two adhesive films

(f) OF_3 without adhesive film

Fig. 13. In-situ strain measurements using FBGs for each optical fibre

As a first analysis, it can be seen that strains within adhesive films (Fig. 13(a)) are extremely dependent on the location of the Bragg gratings. The behaviour of the adhesive at the edge of the plies is the most striking: during the cure, it seems to be able to keep the behaviour proper to its resin. The adhesive is not reinforced with carbon fibres and is thus expected to show thermal expansion during heating and chemical shrinkage during isothermal dwells (as detailed in previous works [36]). However, when the cooling begins, the behaviour of the reinforcement carbon fibres causes significant thermal shrinkage in the composite laminates, constraining the adhesive. It should also be noted that, for all FBG strain measurements within the adhesive, the signal measured by the FO_1 is strongly disturbed for each grating at the beginning of the cure cycle. This disturbance may be due to the migration of the adhesive as detailed in subsection 3.1. The behaviour of the adhesive seems to cause some noticeable strain gradients inside the uncured laminates (Fig. 13 (c) and (e)), especially at the edge of the parts (FBG1 measurements).

Another notable first observation is that, for the specimen without adhesive film (Fig. 13(b)), strains should only be caused by the difference between the cured and uncured prepreg thermomechanical and thermochemical characteristics. However, strains measured at the interface between laminates (cured one and uncured one) suggest that this area is filled with resin and, during the second isothermal dwell at 180°C, noticeable chemical shrinkage is observed. The thermal expansion measured by OF_1 during the cooling ramp is lower than all the expansions recorded by the FBGs of OF_2 and OF_3 during cooling (Fig. 13(d) and (f)). To understand this, images of the interface between the two laminates were obtained using an optical microscope as illustrated in Fig. 14. There seems to be a wider layer of unreinforced matrix at the interface between the initially cured $[0_{20}]$ laminate and the initially uncured one, which is then likely to influence strains measured by the optical fibre. We are carrying on considering that during their autoclave-curing laminates, and this is truer with unidirectional ones, undergo mainly vertical (Z axis) resin flows. This flow (according Z axis) is responsible for a layer of unreinforced resin on the top of the lower laminate (please see Fig. 14) which results, at end of manufacturing process, to resin accumulation at the interface between the two laminates. In other words, this means that the optical fibre OF_1 with its 3 Bragg gratings remains embedded in an unreinforced thick layer of M21EV resin and is strongly influenced by the thermomechanical behaviour of the already cured laminate. This can explain why the strains measured by OF_1 during cooling are lower than all the strains measured by OF_2 and OF_3 during cooling and lower than those measured by OF_1 for the co-bonded specimen with two adhesive films.

Some differences are already noticeable between the two specimens, the adhesive has an influence on cure strains. However, to properly analyse the large amount of experimental results obtained using FBGs, further analysis is required. Experimental measurements will therefore be analysed step by step and further discussed below.

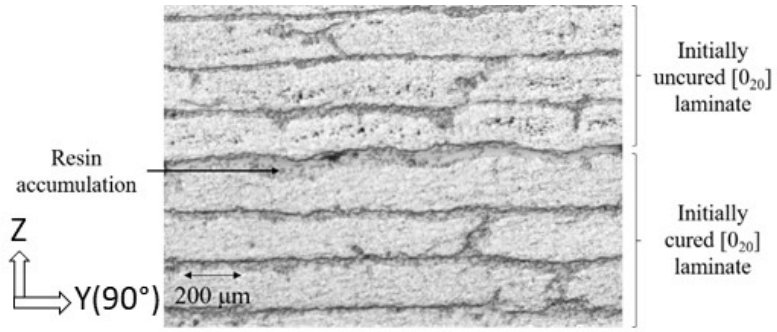

Fig. 14. Optical microscope imaging of the cured/uncured laminate interface after co-bonding without adhesive

4.4. Results analysis at the edge of co-bonded specimens

Firstly, changes in strains at the edge of the assemblies are analysed according to the curing time. Measurements made by FBG1s of each optical fibre are compared and illustrated in Fig. 15 for both specimens; with (Fig. 15(a)) and without (Fig. 15(b)) adhesive film. To facilitate the analysis, measurements before gelation, where the continuity of material/optical fibre displacements is not guaranteed, were removed and strains were reset to 0 at the gel point of the prepreg, i.e. at the beginning of the first isothermal dwell (see Fig. 12). For a better understanding of the different phenomena involved, strains were also plotted against temperature, as illustrated in Fig. 16.

On the edge, both specimens are influenced by the resin located at the interface, be it the adhesive or the excess of M21EV resin. Strain gradients are therefore visible for both types of co-bonding, especially during cooling.

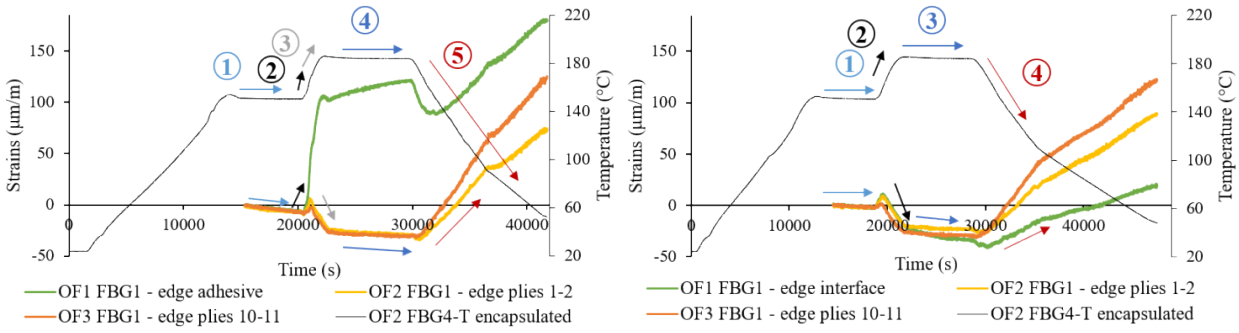

(a) With two adhesive films (b) Without adhesive film

Fig. 15. Strain measurements using FBG1s at the edge of both specimens plotted versus time

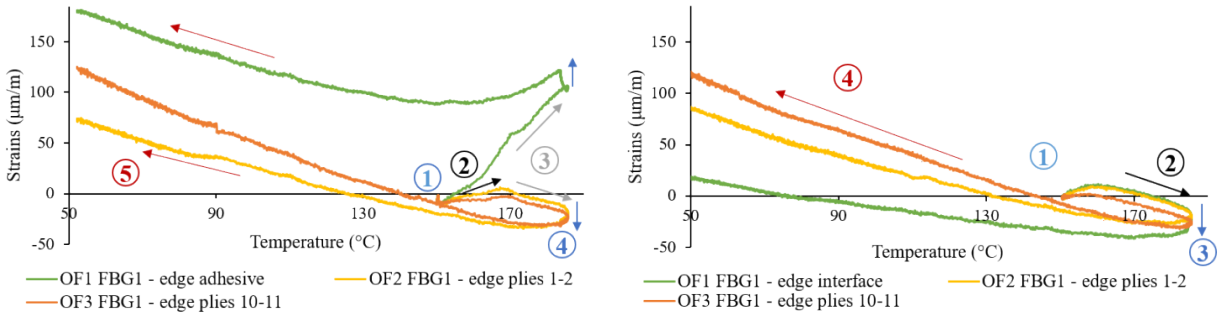

(a) With two adhesive films (b) Without adhesive film

Fig. 16. Strain measurements using FBG1s at the edge of both specimens plotted versus temperature

Strains obtained for the specimen with two adhesive films are illustrated in Fig. 15(a) and Fig. 16(a), measurements postponed to 0 begin with the first isothermal dwell (zone 1 in Fig. 15(a) and Fig. 16(a)), during which slight chemical shrinkage is observed within the adhesive films. This chemical shrinkage also results in strains being lowered in the prepreg. The second heating ramp then starts (zones 2 and 3 in Fig. 15(a) and Fig. 16(a)) and, while the adhesive expands thermally, the prepreg shrinks in the direction parallel to the carbon fibres. Strain evolution during this heating ramp can be divided into two zones: zone 2, where the thermal expansion of the adhesive is predominant and causes strain gradients measured by FO_2 and FO_3; and zone 3, where the thermal shrinkage of carbon fibres becomes predominant within the laminate. The transition from zone 2 to zone 3 corresponds to the glass transition temperature of the adhesive being passed (see Fig. 12). The thermal expansion of the adhesive measured by FO_1 increases with the transition to the rubbery state. This passing of the glass transition temperature is also accompanied by a decrease of the mechanical properties of the adhesive, which may explain the change of behaviour within the laminate. During the second isothermal dwell (zone 4 in Fig. 15(a) and Fig. 16(a)), the fully crosslinked adhesive does not present chemical shrinkage and its strains increase slightly, probably due to a relaxation phenomenon. Finally, the cooling begins (zone 5 in Fig. 15(a) and Fig. 16(a)), the adhesive undergoes thermal shrinkage at the beginning of the thermal ramp, which causes a strain gradient within the prepreg, then the thermal expansion of the carbon fibres becomes predominant and drags the adhesive along.

Strains obtained for the specimen co-bonded without adhesive film are illustrated in Fig. 15(b) and Fig. 16(b). The first notable phenomenon occurs during the second heating ramp (zone 2 in Fig. 15(b) and Fig. 16(b)). A slight thermal expansion is observed at the interface, which leads to strain gradients in the thickness of the laminate. Soon after the start of this thermal ramp, the thermal shrinkage of laminates according the longitudinal direction (i.e. parallel to the fibres) becomes predominant. The thermal shrinkage of the rubbery uncured prepreg is greater than the thermal shrinkage of the cured prepreg. Thus, the further away an area is from the interface with the cured laminate, the greater is its thermal shrinkage. During the isothermal dwell (zone 3 in Fig. 15(b) and Fig. 16(b)) noticeable chemical shrinkage takes place at the interface, confirming the idea that this area is richer in resin. Finally, during cooling, the

lower thermal shrinkage caused by the resin aggregation at the interface between the two laminates causes a strain gradient in the thickness of the laminate.

4.5. Results analysis at a quarter of co-bonded specimens

Strains measured by FBG3 gratings at a quarter of the assemblies are compared and illustrated in Fig. 17 and Fig. 18 for both specimens - with (Fig. 17(a) and Fig. 18(a)) and without (Fig. 17(b) and Fig. 18(b)) adhesive film. As before, to facilitate the analysis, strains were reset to 0 at the gel point of the prepreg, i.e. at the beginning of the first isothermal dwell (see Fig. 12), and strain variations are plotted against time (Fig. 17) and temperature (Fig. 18) to facilitate the analysis of the phenomena involved.

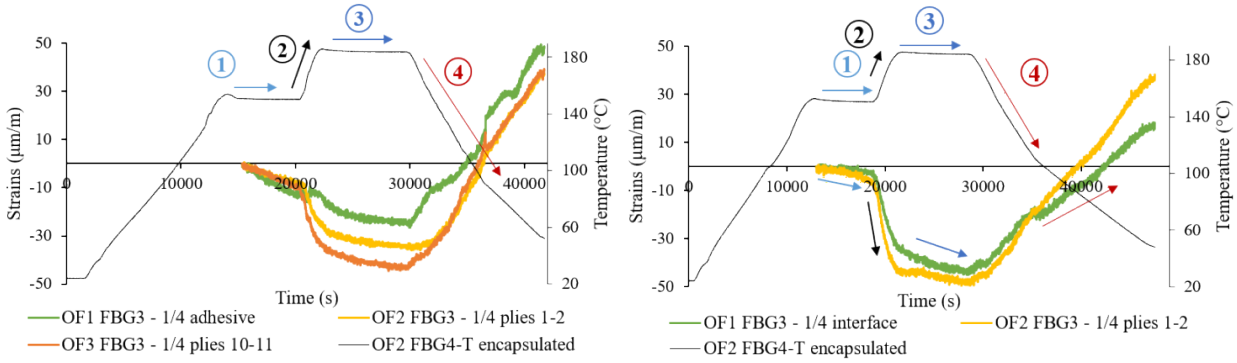

(a) With two adhesive films (b) Without adhesive film

Fig. 17. Strain measurements using FBG3s at a quarter of both specimens plotted against time

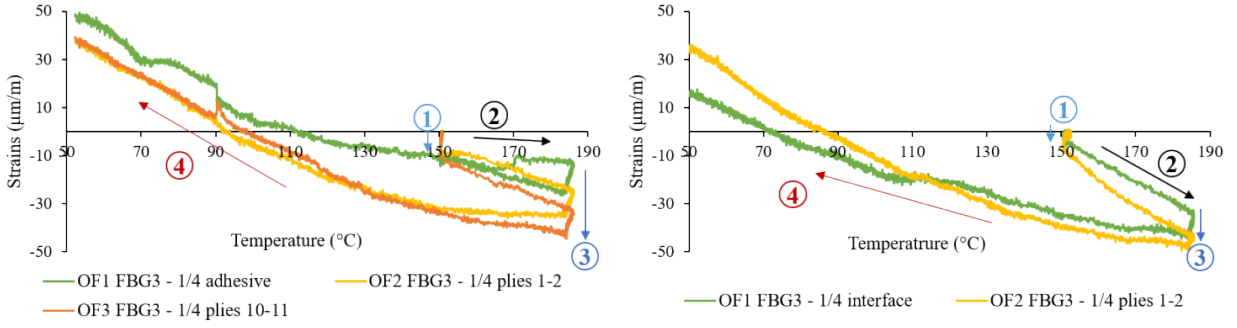

(a) With two adhesive films (b) Without adhesive film

Fig. 18. Strain measurements using FBG3s at a quarter of both specimens plotted against temperature

Strains obtained for the specimen with two adhesive films are illustrated in Fig. 17(a) and Fig. 18(a). FBG3 gratings positioned at a quarter of the assembly reveal an intermediate behaviour between observations made at its centre and at its edge. The evolution of strains measured in adhesive films is closer to the prepreg behaviour; the adhesive is not free to expand thermally and partially follows the thermal shrinkages of carbon fibres. The chemical shrinkage caused by the crosslinking of the adhesive is visible during the first isothermal dwell (zone 1 in Fig. 17(a) and Fig. 18(a)), then strains within the adhesive stabilize. The behaviour of the adhesive generates a strain gradient in the thickness of the uncured laminate. During the second heating ramp (zone 2 in Fig. 17(a) and Fig. 18(a)), plies

of the uncured prepreg shrink. The uncured prepreg is rubbery and the cured prepreg is in a glassy state. The thermal shrinkage is therefore greater in the uncured laminate and strain gradients appear in the thickness of the laminate. The closer the FBG is to the cured laminate the less marked is the thermal shrinkage. This phenomenon is exacerbated by the thermal expansion of the adhesive. During the second isothermal dwell (zone 3 in Fig. 17(a) and Fig. 18(a)), a slight chemical shrinkage can be observed again. During the final cooling (zone 4 in Fig. 17(a) and Fig. 18(a)) the prepreg shrinks thermally. The two laminates reach the cured state, their coefficients of thermal expansion are the same and thermal shrinkages become equivalent in the entire thickness of the laminate.

Fig. 17(b) and Fig. 18(b) illustrate the strain development in the thickness of the assembly co-bonded without adhesive film. As seen above, due to various incidents, only optical fibres FO_1 and FO_2 are studied. The evolution of strains follows the same phenomena as at the centre of the assembly. However, these phenomena are exacerbated and cause larger strain gradients. The interface does not undergo significant chemical shrinkage. During the first isothermal dwell (zone 1 in Fig. 17(b) and Fig. 18(b)) it is the slight chemical shrinkage of the uncured laminate that induces a strain gradient. During the second heating ramp (zone 2 in Fig. 17(b) and Fig. 18(b)) the effect of the rubbery thermal shrinkage of the uncured laminate accentuates the gradient already initiated during the first isothermal dwell. During the second isothermal dwell (zone 3 in Fig. 17(b) and Fig. 18(b)) the effect of chemical withdrawal increases. Finally, cooling down begins (zone 4 in Fig. 17(b) and Fig. 18(b)). Once again, the thermal shrinkage of the interface is reduced in comparison with the measurements made in the laminate.

4.6. Results analysis at the centre of co-bonded specimens

Finally, strain evolutions at the centres of assemblies are analysed. Measurements made by FBG2s of each optical fibre are compared and illustrated in Fig. 19 and Fig. 20 for both specimens - with (Fig. 19(a) and Fig. 20(a)) and without (Fig. 19(b) and Fig. 20(b)) adhesive film. As before, to facilitate the analysis, strains were reset to 0 at the gel point of the prepreg, i.e. at the beginning of the first isothermal dwell (see Fig. 12), and strain variations are plotted against time (Fig. 19) and temperature (Fig. 20) to facilitate the analysis of the phenomena involved.

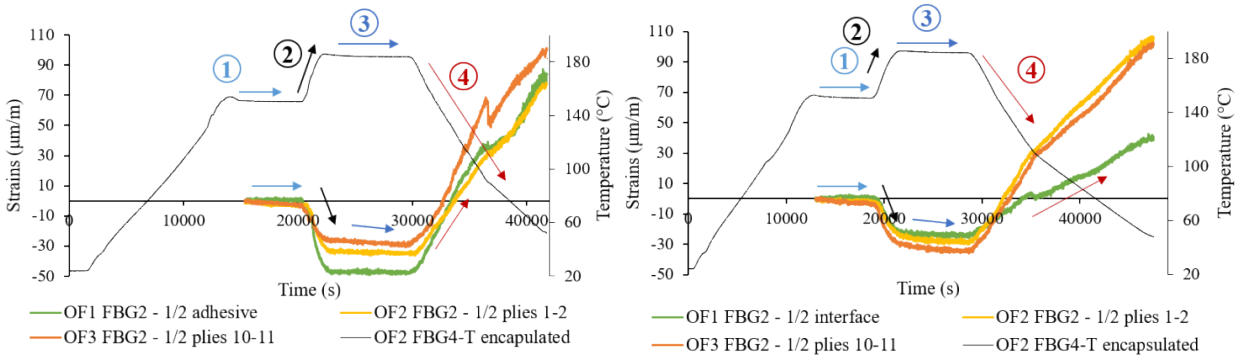

(a) With two adhesive films (b) Without adhesive film

Fig. 19. Strain measurements using FBG2s at the centre of both specimens plotted against time

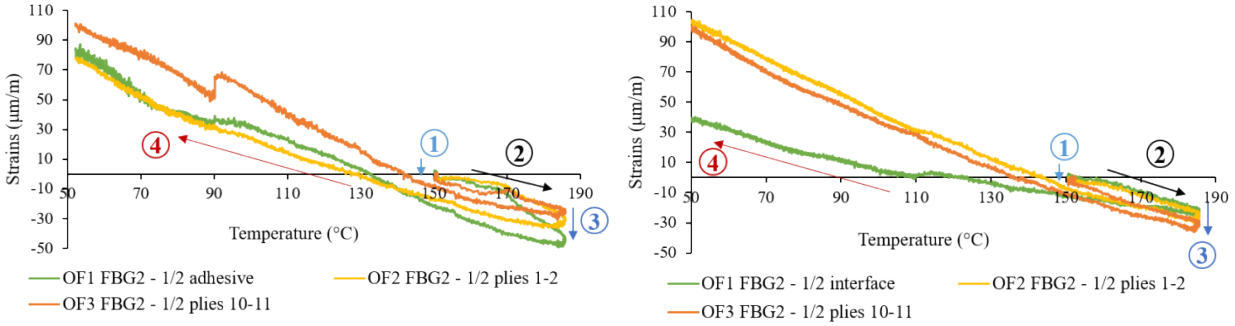

(a) With two adhesive films (b) Without adhesive film

Fig. 20. Strain measurements using FBG2s at the centre of both specimens plotted against temperature

Strains measured by FBG2 gratings at the centre of the specimen co-bonded with adhesive films are illustrated in Fig. 19(a) and Fig. 20(a). The results obtained are different from observations made at the edge and at a quarter of the specimen. The adhesive exhibits a behaviour that seems close to that of the cured prepreg in the direction of the carbon fibres. In this area of the assembly, positioned in the centre of the parts, the adhesive is strongly influenced by the composite laminates that enclose it. However, the observed gradient is opposite to the one measured at a quarter of the parts. The shrinkage of the adhesive generates a strain gradient in the thickness of the laminate. During the second isothermal dwell and the cooling down (zones 3 and 4 in Fig. 19(a) and Fig. 20(a)), the low chemical shrinkages and the thermal shrinkage are led by the glassy behaviour of the prepreg.

Strains measured by FBG2 gratings at the centre of the specimen co-bonded without adhesive film are illustrated in Fig. 19(b) and Fig. 20(b). Compared to the measurements made at the edges of the parts, the interface does not undergo significant chemical shrinkage. As explained above, the strain behaviour is quite similar to measurements obtained at a quarter of the parts. During the first isothermal dwell (zone 1 in Fig. 19(b) and Fig. 20(b)), the slight chemical shrinkage of the uncured laminate induces a strain gradient. During the second heating ramp (zone 2 in Fig. 19(b) and Fig. 20(b)) the difference of coefficient of thermal expansion between the rubbery uncured laminate and the glassy cured laminate increases this strain gradient. During the second isothermal dwell (zone 3 in Fig. 19(b) and Fig. 20(b)) the effect of chemical shrinkage increases. Finally, the cooling begins (zone 4 in Fig. 19(b) and Fig. 20(b)). Both laminates are then glassy, fully cured materials and their coefficients of thermal expansion are the same. The accumulation of resin once again reduces the thermal shrinkage at the interface.

Strain gradients in the thickness of the assembly at the centre of the parts thus differ between the cases with and without adhesive film. Without adhesive film, the coefficient of thermal expansion of the rubbery uncured laminate is greater than that of the glassy crosslinked laminate and the plies farther from the interface contract more during the second heating ramp. This phenomenon is faint at the edges of the parts and starts to be significant in their centres, but it is at a quarter of the parts that it has the most impact. As seen above, in the case of the specimen co-bonded with adhesive films, strain behaviours are quite similar during the second heating ramp at a quarter and at the edge of

a part. However, strain gradients generated at the centres of the parts are quite different; in the case of co-bonding with adhesive, the shrinkage during the thermal ramp increases as it approaches the interface.

These deformation measurements highlight many phenomena and show that the adhesive has an influence on the development of strains during curing.

4.7. Post-cure behaviour and coefficients of thermal expansion validation

To validate the consistency of the monitoring method using FBGs in situ, post-cure measurements were made on the co-bonded specimen with adhesive films and were compared with the coefficient of thermal expansion of the glassy laminates obtained by TMA measurements. After the autoclave curing and bonding, the assembly was demoulded and subjected to heating from 20°C to 190°C inside the autoclave, with a heating ramp of 2°C/min. FBG measurements were used to study the post-curing temperature behaviour and to compare the strain monitoring with the coefficient of thermal expansion measured by TMA on cured specimens. The results obtained are plotted against time for each optical fibre in Fig. 21 and against temperature for each FBG position in Fig. 22.

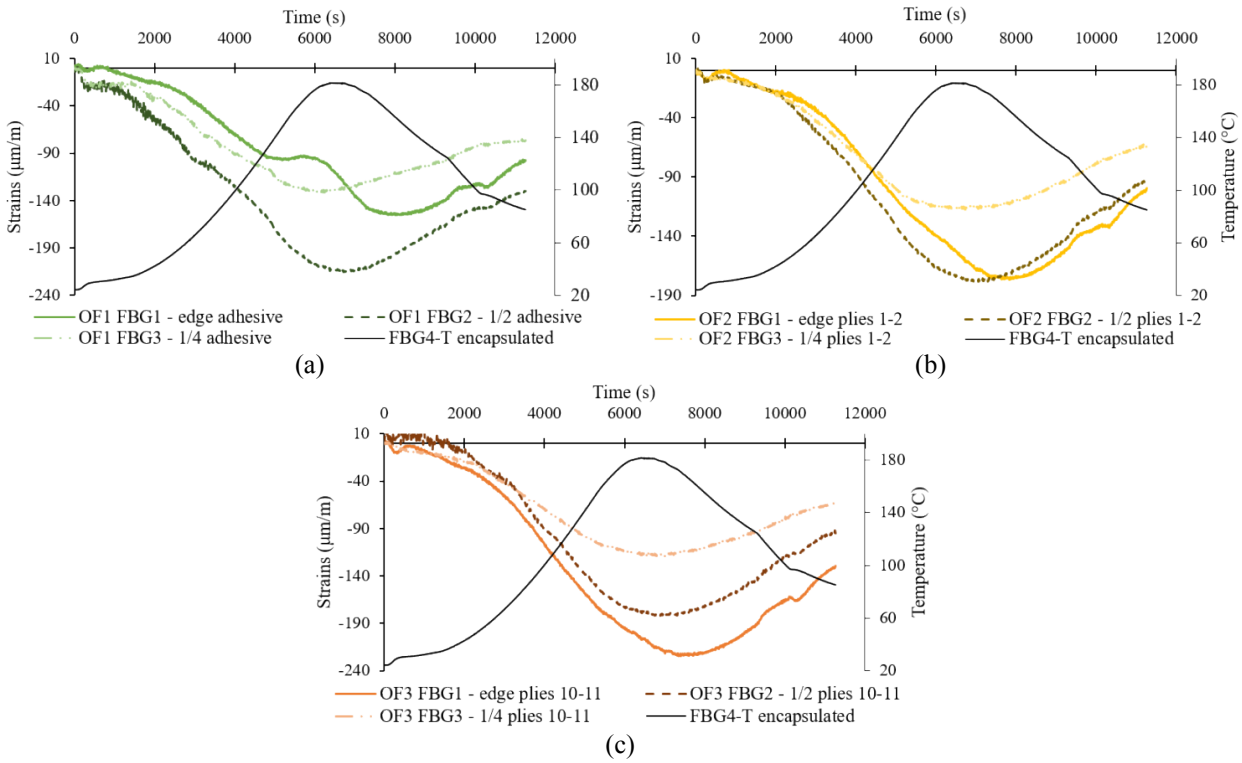

Fig. 21. Comparison of strain measurements plotted against time for each optical fibre during a post-cure thermal ramp on the co-bonded sample with adhesive films

The comparison of strains measured at the edge of the specimen is illustrated in Fig. 22(a). The strain gradients observed during the bonding cycle are also visible during this post-cure ramp. The adhesive exhibits behaviour that is intermediate between the thermal shrinkage of the adjacent prepreg and its own thermal expansion. A change of slope is observed as the glass transition temperature is reached: the coefficient of thermal expansion being higher in

the rubbery state than in the glassy state, the thermal expansion of the adhesive generates a strain gradient within the laminate. Coefficients associated with thermal shrinkages can be deduced from FBG measurements. The coefficient obtained between plies 10 and 11 corresponds to 98% of the coefficient of thermal expansion of the prepreg in the glassy state measured by TMA. Those measured between plies 1 and 2 and at the level of the adhesive films before the glass transition temperature was passed correspond to 74% of the coefficient of thermal expansion at the glassy state of the prepreg. The adhesive therefore limits the thermal strains of the laminate, even when the cure is complete.

Fig. 22(b) and Fig. 22(c) illustrate the evolution of strains at the centre and at a quarter of the parts. Strains measured between plies 1 and 2 and between plies 10 and 11 are almost the same. However, measured strains diverge from the coefficient of thermal expansion measured by TMA, especially for strains measured by FBG3 placed at a quarter of the parts. The adhesive film presents greater shrinkage than laminate. This confirms the measurements obtained during the bonding cycle at the centre of the parts, in which the adhesive films exhibited greater shrinkage during the thermal ramps than the laminate did.

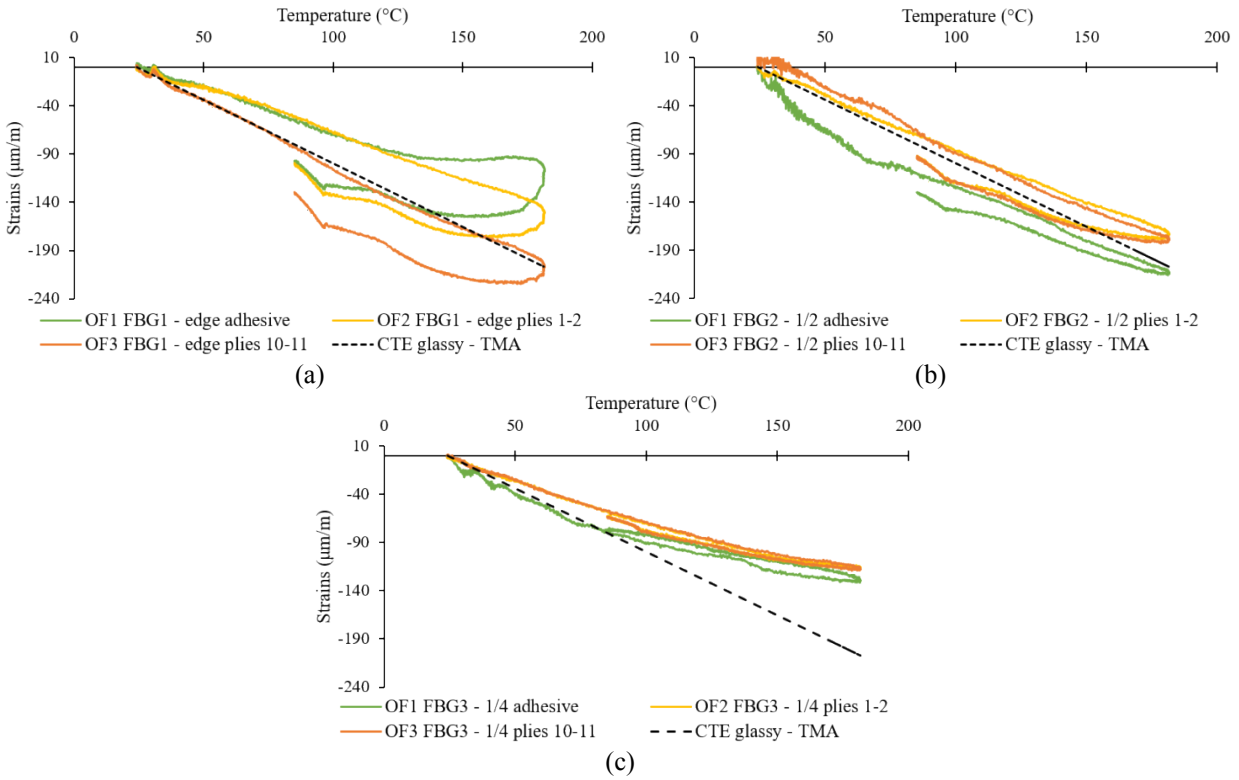

Fig. 22. Comparison of strain measurements plotted against temperature for each FBG position during a post-cure thermal ramp on the co-bonded sample with adhesive films

5. Conclusion and prospects

A new and significant experimental investigation has been carried out to properly understand the behaviour of the adhesive and its influence on process-induced strains during autoclave bonding of composite substrates. The

experiments reveal an unexpected, complex behaviour of the adhesive, proving that adhesive films cannot be ignored if we are to properly understand and anticipate process-induced strains of integrated structures.

Post-cure distortion measurements, micro-tomography, and FBG in-situ monitoring conducted during this research work furnish a strong experimental basis for a better understanding of the bonding processes and the phenomena involved. The main information obtained from these investigations concerns the effects of adhesive migration on the properties of the uncured composite substrates, considering the impact of the bonding process selected and the influence of the number of adhesive films used on the final distortions of assemblies, and, finally, provides complete in-situ measurements of strain developments during a co-bonding process with and without adhesive.

These experimental data also show that wise selection of the bonding process, of the number of adhesive films and of the composite substrate stacking can enable cure distortions to be greatly reduced. The co-curing process which can generate important warpage for perfectly symmetrical thin co-cured samples may also be the best choice for thick assemblies. In the same way, increasing the number of adhesive films will reduce the warpage of thick co-bonded assemblies but will also probably increase the process-induced distortions of thin co-cured assemblies. The optimisation of the bonding process will presumably have to be achieved through simulation.

This research provides a strong base on which to develop a simulation tool to predict the process-induced strains during bonding. It proves that the adhesive films and their complex behaviour cannot be ignored if a solid virtual manufacturing tool is to be developed. Some attempts to simulate bonding processes are available in [41]. The FEA model developed [9,41] can simulate the thermo-mechanical behaviour of both materials but ignores the resin flow. Such a model cannot take account of all the phenomena involved during the cure of bonded assemblies, such as the resin migration of the adhesive. Identifying the precise impact of the migration of the adhesive on the properties of the uncured prepreg plies is essential, especially for thin assemblies. A model taking account of the resin flow or, a semi-empirical model taking account of the evolution of the prepreg properties with the migration of the adhesive could allow to predict the process-induced strains of bonded composite parts more accurately.

Acknowledgements

This research work was undertaken as part of the MAESTRIA project of CORAC - Conseil pour la Recherche Aéronautique Civile, supervised and founded by the DGAC - Direction Générale de l'Aviation Civile and as a part of a partnership with Dassault Aviation.

References

[1] D. Stefaniak, E. Kappel, T. Spröwitz, C. Hühne, Experimental identification of process parameters inducing warpage of autoclave-processed CFRP parts, Composites Part A: Applied Science and Manufacturing. 43 (2012) 1081–1091. https://doi.org/10.1016/j.compositesa.2012.02.013.

[2] M. Fiorina, A. Seman, B. Castanie, K.M. Ali, C. Schwob, L. Mezeix, Spring-in prediction for carbon/epoxy aerospace composite structure, Composite Structures. (2017). https://doi.org/10.1016/j.compstruct.2017.02.074.
[3] L. Mezeix, A. Seman, M.N.M. Nasir, Y. Aminanda, A. Rivai, B. Castanié, P. Olivier, K.M. Ali, Spring-back simulation of unidirectional carbon/epoxy flat laminate composite manufactured through autoclave process, Composite Structures. 124 (2015) 196–205. https://doi.org/10.1016/j.compstruct.2015.01.005.
[4] I. Baran, K. Cinar, N. Ersoy, R. Akkerman, J.H. Hattel, A Review on the Mechanical Modeling of Composite Manufacturing Processes, Archives of Computational Methods in Engineering. 24 (2017) 365–395. https://doi.org/10.1007/s11831-016-9167-2.
[5] T. Garstka, N. Ersoy, K.D. Potter, M.R. Wisnom, In situ measurements of through-the-thickness strains during processing of AS4/8552 composite, Composites Part A: Applied Science and Manufacturing. 38 (2007) 2517–2526. https://doi.org/10.1016/j.compositesa.2007.07.018.
[6] K. Takagaki, S. Minakuchi, N. Takeda, Process-induced strain and distortion in curved composites. Part II: Parametric study and application, Composites Part A: Applied Science and Manufacturing. 103 (2017) 219–229. https://doi.org/10.1016/j.compositesa.2017.09.019.
[7] E. Kappel, A zone-based approach to predict process-induced distortions of composite structures based on a 'spring-in reference curve,' Composite Structures. 209 (2019) 143–149. https://doi.org/10.1016/j.compstruct.2018.10.045.
[8] G. Fernlund, N. Rahman, R. Courdji, M. Bresslauer, A. Poursartip, K. Willden, K. Nelson, Experimental and numerical study of the effect of cure cycle, tool surface, geometry, and lay-up on the dimensional fidelity of autoclave-processed composite parts, Composites Part A: Applied Science and Manufacturing. 33 (2002) 341–351.
[9] L. Moretti, B. Castanié, G. Bernhart, P. Olivier, Characterization and modelling of cure-dependent properties and strains during composites manufacturing, Journal of Composite Materials. (2020) 002199832091247. https://doi.org/10.1177/0021998320912470.
[10] P. Olivier, J.P. Cottu, Optimisation of the co-curing of two different composites with the aim of minimising residual curing stress levels, Composites Science and Technology. 58 (1998) 645–651.
[11] K.E. Tarsha-Kurdi, P. Olivier, Thermoviscoelastic analysis of residual curing stresses and the influence of autoclave pressure on these stresses in carbon/epoxy laminates, Composites Science and Technology. 62 (2002) 559–565.
[12] T. Curiel, G. Fernlund, Deformation and stress build-up in bi-material beam specimens with a curing FM300 adhesive interlayer, Composites Part A: Applied Science and Manufacturing. 39 (2008) 252–261. https://doi.org/10.1016/j.compositesa.2007.10.019.
[13] D. Djokic, A. Johnston, A. Rogers, P. Lee-Sullivan, N. Mrad, Residual stress development during the composite patch bonding process: measurement and modeling, Composites Part A: Applied Science and Manufacturing. 33 (2002) 277–288. https://doi.org/10.1016/S1359-835X(01)00083-5.
[14] H.S. Kim, S.W. Park, D.G. Lee, Smart cure cycle with cooling and reheating for co-cure bonded steel/carbon epoxy composite hybrid structures for reducing thermal residual stress, Composites Part A: Applied Science and Manufacturing. 37 (2006) 1708–1721. https://doi.org/10.1016/j.compositesa.2005.09.015.
[15] H. Fuchs, K.D. Fernholz, P. Deslauriers, Predicted and Measured Bond-Line Read-Through Response in Composite Automotive Body Panels Subjected to Elevated Temperature Cure, The Journal of Adhesion. 86 (2010) 982–1011. https://doi.org/10.1080/00218464.2010.515471.
[16] F. Groh, E. Kappel, C. Hühne, W. Brymerski, Experimental Investigation of Process Induced Deformations of Automotive Composites with Focus on Fast Curing Epoxy Resins, in: ICCM, Copenhagen, 2015.
[17] C. Liebl, M. Johlitz, B. Yagimli, A. Lion, Three-dimensional chemo-thermomechanically coupled simulation of curing adhesives including viscoplasticity and chemical shrinkage, Computational Mechanics. 49 (2012) 603–615. https://doi.org/10.1007/s00466-011-0663-9.
[18] K.A. Patankar, D.A. Dillard, K.D. Fernholdz, Characterizing the constitutive properties and developing a stress model for adhesive bond-line readout, International Journal of Adhesion and Adhesives. 40 (2012) 149–157.
[19] K. Priesnitz, J. Sinke, R. Benedictus, Influence of the temperature cycle on local distortions in car panels caused by hot curing epoxies, International Journal of Adhesion and Adhesives. 50 (2014) 216–222. https://doi.org/10.1016/j.ijadhadh.2014.01.035.
[20] K. Priesnitz, J. Sinke, R. Benedictus, On the simulation of panel distortions due to hot curing adhesives, International Journal of Solids and Structures. 51 (2014) 2470–2478. https://doi.org/10.1016/j.ijsolstr.2014.03.016.

[21] J. Li, X. Yao, Y. Liu, Z. Cen, Z. Kou, D. Dai, A study of the integrated composite material structures under different fabrication processing, Composites Part A: Applied Science and Manufacturing. 40 (2009) 455–462. https://doi.org/10.1016/j.compositesa.2008.10.022.
[22] C. Dong, A parametric study on the process-induced deformation of composite T-stiffener structures, Composites Part A: Applied Science and Manufacturing. 41 (2010) 515–520. https://doi.org/10.1016/j.compositesa.2009.12.009.
[23] M. Waris, P.-J. Liotier, S. Drapier, Effect of the mold on the residual strain field monitored with optical fibers sensors in resin transfer molding processes, Journal of Composite Materials. 48 (2014) 2589–2601. https://doi.org/10.1177/0021998313501532.
[24] H.-J. Yoon, D.M. Costantini, V. Michaud, H.G. Limberger, J.-A. Manson, R.P. Salathe, C.-G. Kim, C.-S. Hong, In situ simultaneous strain and temperature measurement of adaptive composite materials using a fiber Bragg grating based sensor, in: E. Udd, D. Inaudi (Eds.), San Diego, CA, 2005: p. 62. https://doi.org/10.1117/12.599075.
[25] H.-J. Yoon, D.M. Costantini, H.G. Limberger, R.P. Salathé, C.-G. Kim, V. Michaud, In situ Strain and Temperature Monitoring of Adaptive Composite Materials, Journal of Intelligent Material Systems and Structures. 17 (2006) 1059–1067. https://doi.org/10.1177/1045389X06064889.
[26] L. Khoun, R. de Oliveira, V. Michaud, P. Hubert, Investigation of process-induced strains development by fibre Bragg grating sensors in resin transfer moulded composites, Composites Part A: Applied Science and Manufacturing. 42 (2011) 274–282. https://doi.org/10.1016/j.compositesa.2010.11.013.
[27] M. Mulle, Éprouvettes Technologiques Instrumentées à coeur par Réseau De Bragg pour l'analyse du Matériau composite dans la structure, Ph. D. thesis - Mechanical Engineering, Université Paul Sabatier - Toulouse III, 2007. https://www.theses.fr/2007TOU30242.
[28] M. Mulle, F. Collombet, P. Olivier, Y.-H. Grunevald, Assessment of cure residual strains through the thickness of carbon–epoxy laminates using FBGs, Part I: Elementary specimen, Composites Part A: Applied Science and Manufacturing. 40 (2009) 94–104. https://doi.org/10.1016/j.compositesa.2008.10.008.
[29] B. Qi, M. Bannister, X. Liu, A. Michie, L. Rajasekera, B. Ashton, Response of an embedded fibre bragg grating to thermal and mechanical loading in a composite laminate, in: Materials Forum, Citeseer, 2004: pp. 93–100. http://citeseerx.ist.psu.edu/viewdoc/download?doi=10.1.1.529.8876&rep=rep1&type=pdf (accessed March 4, 2017).
[30] L.P. Canal, R. Sarfaraz, G. Violakis, J. Botsis, V. Michaud, H.G. Limberger, Monitoring strain gradients in adhesive composite joints by embedded fiber Bragg grating sensors, Composite Structures. 112 (2014) 241–247. https://doi.org/10.1016/j.compstruct.2014.02.014.
[31] J. Huang, J. Zeng, Y. Bai, Y. Wang, K. Wang, X. Wu, Z. Cheng, D. Liang, Real-time monitoring for the CFRP/aluminium-alloy bonding structure during curing process using encapsulated fiber Bragg grating sensor, Optical Fiber Technology. 57 (2020) 102216. https://doi.org/10.1016/j.yofte.2020.102216.
[32] FM 300 Epoxy Film Adhesive - Technical Data Sheet, (2013).
[33] M. Bornert, F. Hild, J.J. Orteu, S. Roux. Digital Image Correlation (chapter 6). in: Full-field measurements and identification in solid mechanics. M. Grediac, F. Hild Editors, ISTE, John Wiley publishing company, (2013) 157-190, Mechanical engineering and solid mechanics series, ISBN 978-1-84821-294-7. https://doi.org/ 10.1002/9781118578469.
[34] M.A. Sutton, J.J. Orteu, H. Schreier, Image Correlation for Shape, Motion and Deformation Measurements. Basic Concepts, Theory and Applications. Springer - 2009 - ISBN 978-0-387-78747-3.
[35] Y.J. Rao, In-fibre Bragg grating sensors, Measurement Sciences and Technology, 8 (1997) 355-375.
[36] A.D.Kersey, M.A. Davis, H.J. Patrick, M. Leblanc, K.P. Kooet Al., Fiber Bragg grating sensors, Journal of lightwave Technology, 15 (1997) 1442-1463.
[37] J.A. Guemes, J.M. Menéndez, Response of Bragg grating fiber-optic sensors when embedded in composite laminates, Composites Science and Technology, 62 (2002) 956-966.
[38] S. Minakuchi, S. Niwa, K. Takagaki, N. Takeda, Composite cure simulation scheme fully integrating internal strain measurement, Composites Part A: Applied Science and Manufacturing. 84 (2016) 53–63. https://doi.org/10.1016/j.compositesa.2016.01.001.
[39] H.-K. Kang, D.-H. Kang, C.-S. Hong, C.-G. Kim, Monitoring of fabrication strain and temperature during composite cure using fiber optic sensor, in: G.Y. Baaklini, E.S. Boltz, S.M. Shepard, P.J. Shull (Eds.), Newport Beach, CA, 2001: p. 211. https://doi.org/10.1117/12.435569.

[40] M. Mulle, F. Collombet, P. Olivier, R. Zitoune, C. Huchette, F. Laurin, Y.-H. Grunevald, Assessment of cure-residual strains through the thickness of carbon–epoxy laminates using FBGs Part II: Technological specimen, Composites Part A: Applied Science and Manufacturing. 40 (2009) 1534–1544.
[41] L. Moretti, Simulation des distorsions de cuisson de pièces composites élaborées par co-bonding en autoclave, Ph. D. thesis - Mechanical engineering, mechanics of materials, IMT - Mines Albi Carmaux, 2019. http://www.theses.fr/2019EMAC0009.

Laure MORETTI: Formal analysis, Investigation, Methodology, Validation, Writing original draft, Writing and editing revised version

Philippe OLIVIER: Writing original draft, Supervision, Validation, Writing and Editing revised version

Bruno CASTANIE: Writing original draft, Supervision, Validation,

Gerard BERNHART: Resources, Funding acquisition, Supervision